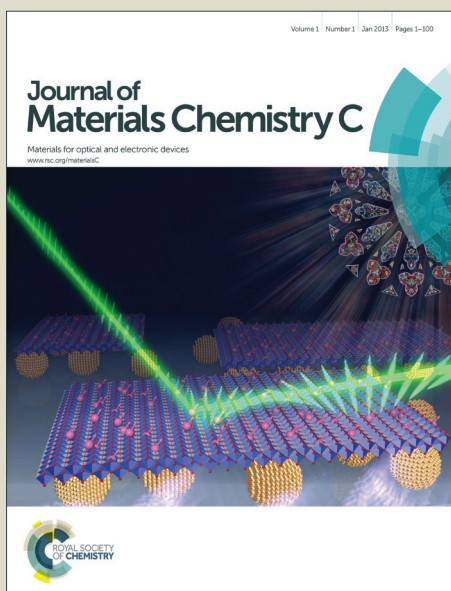


Journal of Materials Chemistry C

Accepted Manuscript



This is an *Accepted Manuscript*, which has been through the Royal Society of Chemistry peer review process and has been accepted for publication.

Accepted Manuscripts are published online shortly after acceptance, before technical editing, formatting and proof reading. Using this free service, authors can make their results available to the community, in citable form, before we publish the edited article. We will replace this *Accepted Manuscript* with the edited and formatted *Advance Article* as soon as it is available.

You can find more information about *Accepted Manuscripts* in the [Information for Authors](#).

Please note that technical editing may introduce minor changes to the text and/or graphics, which may alter content. The journal's standard [Terms & Conditions](#) and the [Ethical guidelines](#) still apply. In no event shall the Royal Society of Chemistry be held responsible for any errors or omissions in this *Accepted Manuscript* or any consequences arising from the use of any information it contains.

Bane to boon: Tailored defect induced bright red luminescence from Cuprous Iodide nanophosphors for *on-demand* rare earth free energy saving lighting applications

Subhajit Saha,[†] Swati Das,[‡] Dipayan Sen,[‡] Uttam Kumar Ghorai,[†] Nilesh Mazumder,[‡] Bipin Kumar Gupta,[‡] and Kalyan Kumar Chattopadhyay*

[†]School of Materials Science and Nanotechnology, Jadavpur University, Kolkata-700032, India,

[‡]Department of Physics, Jadavpur University, Kolkata-700032, India,

[‡]National Physical Laboratory (CSIR), Dr. K. S. Krishnan Road, New Delhi 110012, India

*Address correspondence to: kalyan_chattopadhyay@yahoo.com

Abstract

The long standing controversy of defect band in cuprous iodide (CuI) has been addressed in this paper from the technological point of view of its solid state lighting application. Recently, solid state lighting technology by using nanophosphor has been proposed as the prime candidate in the energy saving lighting paradigm. Here we demonstrate a novel rare earth free and nontoxic CuI nanophosphor which has been synthesized by facile solvothermal route. These nanophosphors are able to show ultra-bright and stable red emission under near UV excitation. The spectral features of this easily derived nanophosphor are not less than any rare earth and cadmium based conventional phosphor. Furthermore, it has been conclusively verified that the deep red emission is strongly related to excess iodine induced optimized defect level engineering in the band structure. The concepts and results presented in this paper clearly establish that CuI

nanophosphor is a promising ‘green’ material for state-of-the-art rare earth free lighting and display applications.

Keywords: CuI, nontoxic, rare earth free, nanophosphor, luminescence, density functional theory

1. Introduction

The developing and highly dynamic field of advanced solid state lighting has lately established itself as one of the major focus of material research owing to several practical and environmental concerns ranging from enhancing energy efficiency to throttling CO₂ emission.¹ Solid state lighting technology by using white light-emitting diodes (WLEDs) are now being deployed regularly due to their low power consumption, long lifetime and fast response time which are actively and significantly shrinking global power requirements and consequently the use of fossil fuels.²⁻⁴ Current development in this field offers a choice between two different routes to design WLEDs. The former one combines three primary colors: red, green and blue (RGB) InGaN LEDs to generate a white light with excellent color gamut. However, relative lower efficiency of green LEDs and different operating circuits of each individual RGB LED result in poor price to performance ratio. An energetically and economically more efficient approach is to down convert the UV or blue light by means of a phosphor (or group of phosphors), such that they can collectively generate white light. Unfortunately these WLEDs suffer from some serious drawbacks such as lower color rendering index due to poor efficiency of the red phosphor counterpart.^{5, 6} So far, only a few red phosphors are available that can be excited by low energy. Hence recently consolidated efforts have been devoted to develop highly-luminescent red phosphors having superior spectral qualities that can be activated in near UV region.

Doping of rare-earth (RE) Eu^{3+} ions in a suitable host is traditionally the most popular protocol to achieve excellent red phosphors.⁷⁻⁹ The choice of this model originated from the notion that when Eu^{3+} occupies a noncentrosymmetric crystallographic site in the host lattice, it shows strong characteristic red emission ($\lambda \sim 615$ nm) because of $^5\text{D}_0 \rightarrow ^7\text{F}_2$ f-f transition.¹⁰ However, production of these RE based phosphors not only requires high temperatures and pressures but also the use of RE ions as luminescence centers exponentially increases the manufacturing cost of the device due to elemental scarcity.^{11,3, 12} Further extensive and in depth search has unveiled highly luminescent red-light emitting CdSe or CdTe quantum dots as an alternative approach that might procure some advantages when comparing with the traditional RE based red phosphors. Despite of their conceived advantages, Cd based quantum dots comes with inherent high level of toxicity even at relatively low concentrations, which significantly hinders their usage in a practical scenario.¹³⁻¹⁵ Therefore, designing an environment friendly nanophosphor at relatively low temperatures which does not incorporate any rare-earth ion currently constitutes a 'Holy Grail' for WLED applications.

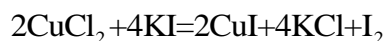
Herein we take the liberty of introducing a novel RE free highly luminescent nanophosphor, Cuprous Iodide, (CuI) whose luminescence properties are equally comparable with the conventional red phosphors. Due to the advent of high excitonic binding energy, (62 meV) previous reports of CuI are predominantly focused on their room temperature free excitonic emissions.^{16, 17} Most of these studies pay attention towards the inter band defect state elimination in CuI for their possible application in near UV excitonic LEDs. In this paper, for the very first time we are going to demonstrate, precise modulation of the defect band inside the band structure of nanocrystalline CuI yields ultra-bright visible luminescence in deep red region. In the current work, a facile solvothermal route for the synthesis of nanocrystalline CuI phosphors is presented.

It is revealed that forced incorporation of excess iodine in the CuI lattice results in defect center mediated strong red emission, which has also been substantiated by first principle calculations using atomistic density functional theory (DFT). DFT results indicate that intentional incorporation of interstitial iodine reduces the Cu-I bond length which facilitates the formation of interband states through mixing of p, d states with s orbital. This study puts light on the origin of defect level emission in CuI which is still under debate in the literature. The resulting ultra-bright red luminescence will promote CuI as a rare earth free, environmentally safe nanophosphor for solid state lighting technology based on WLEDs.

2. Results and discussion

2.1 Structural and compositional analysis

We have carried out detail investigation of structural and photo physical properties of the developed CuI nanophosphors at various stages of solvothermal synthesis to study the effect of excess iodine on different physical parameters. Initially white precipitate CuI crystals are formed in the solution via following reaction-



Due to the presence of excess iodine, the solution was initially brown just before placing it in the autoclave. But, after 12 hour of reaction in a closed system, the solution became absolutely transparent (illustrated clearly in Figure S1, electronic supplementary information). This phenomenon definitively indicates that excess dissolved iodine in the reaction medium has been incorporated in the precipitated CuI due to application of high temperature and pressure. Confirmation of phase purity of the obtained products was carried out by X-ray diffraction (XRD) analysis. The typical XRD pattern of the synthesized nanophosphors (shown in Figure 1(a)), clearly reveals that all diffraction peaks can be assigned to a cubic phase γ -CuI

[JCPDS#06-0246]. The well assigned sharp diffraction peaks with no other unwanted signals confirm the phase purity of the products along with their highly crystalline nature.

A closer observation to (111) XRD peak (shown in in Figure 1(b)) discloses the gradual lower angle shift of the peak position with the increase in reaction time. Generally, such a shift in the XRD pattern is the result of unit cell expansion caused by the substitution of larger atoms in the lattice.^{18, 19} Similarly, in the current case, the incorporation of excess iodine in the CuI lattice is responsible for the increase in the unit cell volume as well as the consequent lower angle shift in XRD pattern. The consistent variation of lattice parameter and unit cell volume (calculated from the XRD data) with the reaction time (shown in Figure S2 of ESI) clearly supports this logic. Since the expansion of unit cell is always associated with a tensile strain, the occurrence of the proposed mechanism has been cross checked by analyzing the induced lattice strain calculated from the Williamson-Hall plot which is shown in Figure S3 (in ESI).²⁰ The trace of increasing lattice strain is clearly evident from continuous increase in the slope of the straight lines with reaction time. Signature of uniform and regular narrow size distribution of these crystals within the nanometric region is prominent from the FESEM and TEM image as shown in Figure 1(c) and 1(d), respectively.

Further investigations of the exact chemical states of the constituent elements within the synthesized nanophosphors were carried out by detailed XPS analyses. All the core level spectra have been charge corrected by taking the peak of C 1s at 284.6 eV, which appeared due to the presence of adventitious carbon on the surface of the samples during atmospheric exposure. The presence of Cu and I with no other impurity peaks in the typical survey scan (shown in Figure S4(a)) reflects the pure phase realization of CuI. The high resolution core level spectra for Cu 2p [shown in Figure 2(a)] consists of two peaks at 952.1eV and 932.2 eV, which corresponds to Cu

$2p_{1/2}$ and Cu $2p_{3/2}$, respectively. The absence of any shake-up satellite peak in all the Cu 2p core level spectra strongly claims the +1 oxidation state of Cu, which is the basic requirement for CuI formation. The peaks located at 619.7 eV and 631.2 eV [shown in Figure 2(b)], are well consistent with I $3d_{5/2}$ and I $3d_{3/2}$ core level spectra of I^- , respectively. Moreover, both the spin orbit splitted peaks of Cu 2p and I 3d are fitted very well with only one component (shown in Figure S4 (b&c)) which reflects the presence of only one valence state of the corresponding elements.

A careful inspection to the high resolution spectra of Cu 2p and I 3d clearly reveals that all the spectra are not exactly in the same binding energy position for all the synthesized nanophosphors, rather a little shift in their binding energy can be observed. The lower binding energy shift, along with the increased intensity of the I 3d peaks for 12 hr. solvothermal treated samples, can be directly attributed to the presence of excess iodine in the corresponding nanophosphors.^{21, 22} At the same time a small higher binding energy shift can be noticed in Cu 2p peaks for 12 hr. solvothermal treated samples. Incorporation of excess I^- in the crystal reduces electron density around Cu which in turn increases the binding energy value in the core level spectra.²³ Detail compositional analysis of the CuI nanophosphors synthesized at different solvothermal reaction time has also been carried out by studying their corresponding EDX (Energy Dispersive X-ray) spectra which is shown in Figure 2(c). EDX spectra clearly indicates the gradual increase in the I content within the nanocrystals with the increase in the reaction time and the ratio of Cu:I reaches to a maximum of 1:1.12 for the samples synthesized at 12 hr. of solvothermal reaction. Hence, the presence of excess iodine in the synthesized nanophosphors is again confirmed by these EDX results.

2.2 Luminescence study and DFT analysis

In order to study the effect of iodine incorporation on the optical properties, room temperature photoluminescence (PL) spectra of the CuI nanophosphors has been studied as a function of reaction time which is presented in Figure 3(a). The individual maxima in excitation/emission intensity were used to record the emission/excitation spectra. The excitation maximum is located at 397 nm (shown in Figure S5 of ESI) which is one of the major excitation source by the LED chips. The emission spectra primarily consist of two peaks; one weak peak ~ 421 nm and a broad peak centered at 688 nm. The higher energy weak peak can be directly ascribed to near band edge emission (NBE).¹⁶ Although, the microscopic origin of the broad emission band remains unclear till date,^{24, 25} the general consensus is that defect level mediated radiative recombination is responsible for the appearance of this red emission band. While the intensity of defect level emission (DLE) increases gradually with reaction time, the NBE remains almost unaltered. The presence of strong DLE with higher reaction time clearly demonstrates that those nanophosphors are very susceptible to various intrinsic defects, interstitials, which form new energy levels and screen the NBE emission. Moreover, these defects are generally distributed in the nanophosphors bodies. Experimental verification of this fact and the signature of previously explained induced lattice strain in the nanophosphors can be realized straight through HRTEM analysis shown in Figure 3(b). HRTEM images of the nanophosphors taken at two terminating point of the synthesis illustrate the difference between lattice fringe patterns of the corresponding (111) planes. Initially, before putting into the autoclave the as obtained samples were characterized by their highly crystalline nature with uniform well resolved lattice fringes having interatomic spacing 0.345 nm. Consequently, the PL spectra of this samples show feeble DLE with a relatively stronger NBE emission. But, due to advent of high pressure in solvothermal reaction, forced introduction of excess iodine in the CuI crystal not only leaves the marks of defect

induced lattice strain in the lattice fringes but also enhances the DLE of the corresponding samples. Signature of this defect induced lattice strain is distinctly detected by the high density of fault regions in the lattice fringes with slightly higher inter atomic spacing (~ 0.351 nm). This type of phenomenon is already supported by earlier reports with different nanophosphors, which show that introduction of defect may distort the lattice fringes leading to the enhancement of DLE.²⁶ Moreover, calculated total density of states (TDOS) (shown in Figure 3(c)) clearly demonstrate the appearance of impurity band near conduction band minima in iodine incorporated samples. Recombination of electrons in the conduction band and holes in the valence band generates the NBE. But, when the electrons from those impurity levels recombine with the holes in the valence band, DLE takes place. Since, the density of DLE is directly proportional to the density of defect states, more and more incorporation of iodine increases these defect states as well as the DLE. The consistency of the PL spectra has been additionally verified by investigating the cathodoluminescence (CL) spectra of the constituent samples which is presented in Figure S6 of ESI. Strong CL emission from the nanophosphors readily proves their potential to be used as field emission display phosphor.

Defect engineering controlled high intensity ratio of DLE to NBE facilitates outstanding photoluminescence properties from these CuI nanophosphors. Enhancement of DLE can be directly evidenced from the digital photograph of the nanophosphors under 365 nm UV lamp (Figure 4 (a)). Upon UV exposure the samples reveal ultrabright red emission whose color coordinate lies in standard red region of CIE chromaticity diagram (shown in Figure 4(b)). Again, from the application point of view it is necessary to obtain phosphor thin films with enriched homogeneity and brightness. Interestingly, when the CuI nano crystals are drop coated and blended on a glass substrate, under UV excitation these highly transparent films show bright

red emission as strong as in the original powder form (shown in Figure 4(c)). Since, Eu^{3+} containing conventional red phosphors emit commonly below 630 nm, it is very difficult to improve the color rendering index in deep-red region by using these phosphors. Hence, WLEDs fabricated by using them also suffers from the embarrassing problem of poor color rendering in deep red region.²⁷ However, broad and intense red emission above 630 nm from the CuI nanophosphors is expected to improve the color rendering in deep red region to a large extent. The PL quantum yield (QY) of these bright nanophosphors has been found to be ~21% in solid condition. It is to be noted that enhanced surface states of the nanocrystals often quenches PL QY in solid form due to partial aggregation and energy transfer mediated nonradiative recombination.^{28, 29} Hence it is very difficult to achieve a high quantum yield of the nanophosphor in solid condition. On the other hand, smaller particle size is also needed to realize higher resolution for the display technology.^{30, 31} Keeping these points in mind a careful survey regarding the PL properties of previous reported red nanophosphors is presented in table 1. From the table, it can be clearly perceived that the emission characteristics of this CuI nanophosphor are not only equally comparable with the already existing red nanophosphors in the literature but also it serves multifold advantages like ecofriendly, nontoxic and stable. The superior spectral characteristics along with uniform PL brightness throughout large area promote this nanophosphor for near-UV activated WLEDs and display applications.

Confirmation of DLE has been justified further by carrying out the time resolved photoluminescence (TRPL) measurement for both the emission wavelength (shown in Figure 5). Detail fitting procedure of the corresponding decay curves along with different decay parameters are depicted in electronic supplementary information. The average lifetime of NBE and DLE was found to be 1.37 ns and 2.82 μs , respectively. Since, any emission originating from defect state

shows longer lifetime than the intrinsic states,³⁶ it is conclusively verified that defect level created by the incorporation of excess iodine in the system generates the red luminescence band. Density functional theory (DFT) calculations have been also carried out to analytically estimate the origin of defect bands in solvothermally grown CuI nanophosphors. Generally, at room temperature, CuI stabilizes in zinc blend like crystal structure. In such a structure, I ions form the cubic closed packed array in which half of the tetrahedral voids are occupied by the Cu⁺ ions and all the octahedral voids remain empty. In a Face Centered Cubic (FCC) lattice, octahedral voids are located at body center position and at the middle of each edges. Hence, in order to achieve our experimental condition some extra iodine atoms would have to be incorporated in the crystal. Since the formation energy of an iodine interstitial at tetrahedral site is much higher than an iodine interstitial at octahedral site³⁷ we opted to introduce extra iodines in these octahedral sites (schematically shown in Figure 6(a)). Corresponding complete supercell structures are supplied as Figure S7 of ESI for reference. Addition of I in the octahedral sites alters the overall electronic properties of the crystal to a great extent which is prominent from the TDOS patterns shown in Figure 3(c). As expected, the TDOS pattern of pure CuI clearly demonstrates two distinct set of bands that are completely separated by a forbidden gap of 3.1 eV which is in excellent agreement with already reported band gap of γ -CuI.^{38, 39} Moreover, the appeared defect band below 0.6 eV from the conduction band minima in I incorporated systems gets stronger and stronger with the introduction of more iodine. In order to figure out the exact orbital contributions that lead to the appearance of this defect band in I incorporated systems, a precise probing of the TDOS curves were carried out by analyzing the partial density of states (PDOS) of different orbitals which are shown in Figure 6(b)-(c). PDOS patterns clearly confirm the well-known notion that majority of the upper valence bands (around -2 to 0 eV) are

dominated by Cu 3d with a noticeable contribution from I 5p whereas the lower edge of the conduction band consists of Cu 4s along with a involvement of I 5s. As the spatial extent of the Cu 3d levels is large and their energies are close to those of the I 5P levels, these orbitals hybridize strongly to generate the valence band. The degree of p-d admixture at the top of the valence band is 0.54 in CuI.⁴⁰ Signature of p-d hybridization is also prominent in both pure and iodine incorporated CuI systems as revealed from Figure 6(b) &(c). Comparison of the PDOS patterns of both the systems readily implies that the localized defect state which appeared in the TDOS pattern of I incorporated CuI structure principally originates due to the major contribution from Cu d and I p orbitals (shown in the inset of Figure 6(c)). But the interesting fact is that, due to introduction of iodine in the octahedral sites, valence band becomes hybridized with the additional contribution from Cu s and I s orbitals which is shown clearly in the right panel of Figure 6(c). Such a mixing of p, d states with s level is the result of stronger overlap of the corresponding orbitals occurred due to the reduction of Cu-I bond length. Initially in pure CuI, the Cu-I bond length was 2.648 Å whereas it changed to 2.553 Å after introduction of octahedral iodine. Moreover, this reduced bond length increases the density of states near the valence band edge due to higher contribution from cation d and anion p levels. This mixing of s level with p, d states are responsible for the appearance of localized defect states below conduction band minima as seen in the TDOS pattern. This type of phenomenon is already supported by earlier reports which show changes in bond length can create new states within the band gap.⁴¹ Moreover; the existence of localized electronic levels near the conduction band can act as traps for excited electrons and is in accordance with the experimentally observed DLE in the room temperature PL spectra of CuI nanophosphors.

After the regular spectroscopic measurements, a prototype device was also constructed by adding CuI nanophosphors over the commercial 395 nm UV LED as represented in Figure 7(a). Under an applied voltage of ~3 Volt, the device glows strongly and a bright red emission comes out (Figure 7(b)). The typical electroluminescence (EL) spectra of the device taken at different applied voltage are shown in Figure 7(c). The position of the EL peaks is very close to their PL counterparts and with the increase in the applied voltage the emission intensity increases gradually. The emission stability of the device was also checked and was found to fluctuate only ~5% for more than 2 hours of operation (shown in Figure S8(e) in ESI). Moreover, no spectral deterioration or appearance of extra peaks in the EL spectra was observed for the samples stored in the ambient conditions for more than 3 months. However, it is observed that, the crystallinity and PL brightness of the nanophosphors decreases slightly after 3 month of synthesis (shown in Figure S8 (a-d)). Due to such long time of atmospheric exposure, the excess iodine present in CuI may easily react with atmospheric oxygen to oxidize it. A small peak corresponding to (002) plane of I_2O_5 [42] also appeared in the XRD pattern (inset of Figure S8 (b)) of the samples carried out after 3 months. This oxidation is readily responsible for the reduction in intensity observed in XRD pattern and PL spectrum. High color quality of the emitted light are demonstrated in CIE chromaticity diagram as shown in Figure 7(d). With the variation of applied voltage shift in the color coordinate was very small. Furthermore, the spectral locus of the emitted radiation lies on the High Definition Television (HDTV) standard color triangle, which strongly claims the color purity in terms of hue and saturation.

3. Conclusions

In summary, highly luminescent and nontoxic CuI nanophosphors have been synthesized by a simple solvothermal route. By increasing reaction time, the synthesized nanophosphors showed

boosted DLE with almost unaltered NBE. The red defect band was so strong that the samples show ultra-bright red emission under UV lamp both in powder and thin film form which could be detected via naked eye. By analyzing the HRTEM images it was confirmed that structurally disordered nanophosphors show enhanced DLE. Those disorders were connected with the corresponding changes in the lattice created by forceful introduction of iodine into the crystal. Further justification of such direct relationship between structural disorder and PL properties was supported by the first principle calculation using Density Functional Theory. DFT results clearly depict evolution of a defect band within the forbidden gap in the interstitial iodine incorporated system. Theoretical calculations indicate that introduction of interstitial iodine not only reduces the Cu-I bond length but also facilitates the formation of interband states through mixing of p, d states with s orbital. The obtained bright red emission with high quantum yield and good color rendering property readily proves the potential of the CuI nanophosphors for using in WLEDs, display and general lighting applications. The present contribution takes a substantial step forward toward the burgeoning interest in the field of environment friendly “rare earth free solid state lighting” application.

Experimental Section:

Synthesis of CuI nanophosphors: CuI nanophosphors have been synthesized by a solvothermal route. Analytical reagent grade $\text{CuCl}_2 \cdot 5\text{H}_2\text{O}$ (Merck, 99.9%), poly-ethylene-glycol (PEG), KI (Merck, 99.9%), Sodium dodecyl sulphate (Merck, 99.9%) and NaNO_3 (Merck, 99.9%) were used as raw materials. The detailed synthesis procedure was as follows-

Initially 0.05 M $\text{CuCl}_2 \cdot 5\text{H}_2\text{O}$ was added in 5mM PEG solution and stirred at 40°C to get a clear solution. In a separate beaker 0.1 M KI and 1.5 mM SDS was mixed in 5mM PEG solution. The mixture was stirred at 40°C till complete dissolution of the SDS in PEG solution and a

transparent solution was obtained. This solution was then added dropwise in the previous solution and stirred at 60°C for 2 hr. till a viscous amaranth solution was obtained. The obtained solution was then added dropwise in a 0.05M NaNO₃ solution and stirred at 60 °C for 2 hr. Finally, tiny CuI crystals precipitated in the solution. This solution along with the precipitate was transferred in 100 ml teflon lined stainless steel autoclave and kept at 180 °C for several hours. After the reaction the autoclave was cooled naturally to room temperature and the precipitate was collected through several times of washing by deionized water and ethanol. Finally the nanophosphors were obtained by oven drying the obtained precipitate.

Instrumentation: Crystallinity and phase purity of the samples were examined by X-ray diffraction (XRD) using Cu *K*α radiation ($\lambda=1.5406 \text{ \AA}$) (D8 Advanced, Bruker). The chemical state of the constituent elements were analyzed by X-ray photoelectron spectroscopy (XPS) using a monochromatic Al *K*α X-ray source ($h\nu = 1486.6 \text{ eV}$) and a hemispherical analyzer (SPECS, HSA 3500). The morphology of the synthesized samples was examined with field emission scanning electron microscope (FESEM Hitachi S-4800), while the crystalline structure of the individual samples was investigated with a high resolution transmission electron microscope (HRTEM JEOL JEM 2100). The UV-Vis transmittance spectra were taken on Shimadzu UV3600 spectrophotometer. The steady state PL spectra were taken by Edinburgh, FLSP-980 spectrofluorometer whereas TRPL measurements were carried out by IBH Fluorocube apparatus (Jobin Yvon-IBH-5000M) and Edinburgh, FLSP-980 luminescence spectrometer. The excitation and emission spectra were corrected for the spectral distribution of the Xe lamp intensity using a reference detector. Long pass optical filters have been used for the elimination of scattered excitation signal in the emission spectra. The photoluminescence quantum yield of the samples were measured by using an integrating sphere whose inner face was coated with

BENFLEC as supplied by Edinburgh instruments. Cathodoluminescence (CL) spectra of the samples were recorded by using Gatan Mono CL equipment attached to the FESEM using a beam accelerating voltage of 5 kV.

Computational details: Our first-principles calculations were performed by CASTEP code which implements a supercell approach to density functional theory. Perdew–Burke–Ernzerhof (PBE) functional within the generalized gradient approximation (GGA) was used to deal with exchange and correlation term. Vanderbilt ultrasoft pseudopotential was used to represent the copper and iodine atoms and plane waves up to energy cut off 450 eV was used in the calculation. Brillouin zone integrations were performed within the Monkhorst Pack scheme using k-point separation of $\sim 0.081 \times 0.081 \times 0.081 / \text{\AA}$. For geometrical optimization, the system was allowed to fully relax using BFGS (Broyden-Fletcher-Goldfarb-Shanno) scheme until the total energy converged to less than 2×10^{-5} eV/atom, the maximum force converged to lower than 0.05 eV/ \AA and the maximum displacement was 0.002 \AA . All calculations were performed in spin unrestricted manner.

To corroborate with the experimental results, two type of CuI structures were considered. For pure CuI system, a $2 \times 2 \times 2$ supercell containing 32 Cu atoms and 32 I atoms was used while to investigate the effect of interstitial iodine one and two iodine was inserted in the octahedral sites. Prior to the calculation of properties all systems were fully optimized in a spin unrestricted manner. A scissors operator of 2.174 eV was used for all electronic properties calculations to compensate for the inherent bandgap related problems associated with DFT.

Acknowledgements

The authors (SS, SD & UKG) acknowledge the financial support from the Council of Scientific and Industrial Research (CSIR), the Government of India, for awarding Senior Research Fellowship during the execution of the work. One of us (DS) wishes to thank the W.B. State Govt. for providing fellowships during the execution of this work. We also wish to thank the Department of Science & Technology (DST), the University Grants Commission for ‘University with Potential for Excellence scheme (UPE-II)’ the Government of India for financial help. Subhajit Saha, Swati Das and Dipayan Sen contributed equally to this work.

Notes and References

†**Electronic Supplementary Information (ESI) available:** Digital images of the precipitated CuI in the solution just before putting into the autoclave and after the hydrothermal reaction, variation of lattice parameter and cell volume with the hydrothermal reaction time, Williamson-Hall plot of the nanocrystals, XPS survey scan, photoluminescence excitation spectra and cathodoluminescence spectra of the CuI nanophosphors, lifetime and decay parameters, 2×2×2 supercell structures of pure and iodine incorporated CuI, EL stability curve of CuI nanophosphors. See DOI: 10.1039/b000000x/:

References:

1. J. Z. Zhang, *The Journal of Physical Chemistry Letters*, 2011, 2, 1351-1352.
2. C. C. Lin, Y. S. Zheng, H. Y. Chen, C. H. Ruan, G. W. Xiao and R. S. Liu, *Journal of The Electrochemical Society*, 2010, 157, H900.
3. C. C. Lin and R.-S. Liu, *The Journal of Physical Chemistry Letters*, 2011, 2, 1268-1277.
4. E. F. Schubert and J. K. Kim, *Science*, 2005, 308, 1274-1278.

5. K.-S. Sohn, D. H. Park, S. H. Cho, J. S. Kwak and J. S. Kim, *Chemistry of Materials*, 2006, 18, 1768-1772.
6. E. Jang, S. Jun, H. Jang, J. Lim, B. Kim and Y. Kim, *Adv Mater*, 2010, 22, 3076-3080.
7. C. Feldmann, T. Jüstel, C. R. Ronda and P. J. Schmidt, *Advanced Functional Materials*, 2003, 13, 511-516.
8. C. Feldmann, *Nanoscale*, 2011, 3, 1947-1948.
9. H. A. Hoppe, *Angewandte Chemie*, 2009, 48, 3572-3582.
10. S. Saha, S. Das, U. K. Ghorai, N. Mazumder, B. K. Gupta and K. K. Chattopadhyay, *Dalton Transactions*, 2013, 42, 12965.
11. T. Ogi, Y. Kaihatsu, F. Iskandar, W.-N. Wang and K. Okuyama, *Advanced Materials*, 2008, 20, 3235-3238.
12. X. Zhang, Y. Zhang, Y. Wang, S. Kalytchuk, S. V. Kershaw, Y. Wang, P. Wang, T. Zhang, Y. Zhao, H. Zhang, T. Cui, Y. Wang, J. Zhao, W. W. Yu and A. L. Rogach, *ACS Nano*, 2013, 7, 11234-11241.
13. M. Dasog, Z. Yang, S. Regli, T. M. Atkins, A. Faramus, M. P. Singh, E. Muthuswamy, S. M. Kauzlarich, R. D. Tilley and J. G. C. Veinot, *ACS Nano*, 2013, 7, 2676-2685.
14. M. J. Anc, N. L. Pickett, N. C. Gresty, J. A. Harris and K. C. Mishra, *ECS Journal of Solid State Science and Technology*, 2012, 2, R3071-R3082.
15. C. Sun, Y. Zhang, Y. Wang, W. Liu, S. Kalytchuk, S. V. Kershaw, T. Zhang, X. Zhang, J. Zhao, W. W. Yu and A. L. Rogach, *Applied Physics Letters*, 2014, 104, 261106.
16. S. Das, S. Saha, D. Sen, U. K. Ghorai and K. K. Chattopadhyay, *Journal of Materials Chemistry C*, 2014, 2, 6592.

17. Z. Zheng, A. Liu, S. Wang, B. Huang, K. W. Wong, X. Zhang, S. K. Hark and W. M. Lau, *Journal of Materials Chemistry*, 2008, 18, 852-854.
18. S. Zeng, G. Ren, C. Xu and Q. Yang, *CrystEngComm*, 2011, 13, 4276.
19. F. Ahmed, S. Kumar, N. Arshi, M. S. Anwar and B. Heun Koo, *CrystEngComm*, 2012, 14, 4016-4026.
20. G. K. Williamson and W. H. Hall, *Acta Metallurgica*, 1953, 1, 22-31.
21. S. Ntais and A. Siokou, *Surface Science*, 2006, 600, 4216-4220.
22. S. Ntais, V. Dracopoulos and A. Siokou, *Journal of Molecular Catalysis A: Chemical*, 2004, 220, 199-205.
23. Y. Cong, J. Zhang, F. Chen and M. Anpo, *The Journal of Physical Chemistry C*, 2007, 111, 6976-6982.
24. A. Gruzintsev, *Journal of Experimental and Theoretical Physics Letters*, 2003, 78, 106-109.
25. (a). M. Gu, P. Gao, X.L. Liu, S.M. Huang, B. Liu, C. Ni, R.-K. Xu and J.-m. Ning, *Materials Research Bulletin*, 2010, **45**, 636-639.
(b). P. Gao, M. Gu, X.L. Liu, B. Liu and S.-M. Huang, *Applied Physics Letters*, 2009, **95**, 221904.
(c). A. N. Gruzintsev and V. N. Zagorodnev, *Physics of the Solid State*, 2012, **54**, 117-122.
(d). G. P. Shevchenko, I. Y. Piskunovich, V. A. Zhuravkov and Y. V. Bokshits, *Inorganic Materials*, 2012, **48**, 630-634.
(e). M. Zi, J. Li, Z. Zhang, X. Wang, J. Han, X. Yang, Z. Qiu, H. Gong, Z. Ji and B. Cao, *physica status solidi (a)*, 2015, DOI 10.1002/pssa.201532015.\

26. H. Li, X. Wang, J. Xu, Q. Zhang, Y. Bando, D. Golberg, Y. Ma and T. Zhai, *Adv Mater*, 2013, 25, 3017-3037.
27. X. Wang, X. Yan, W. Li and K. Sun, *Adv Mater*, 2012, 24, 2742-2747.
28. T. Otto, M. Muller, P. Mundra, V. Lesnyak, H. V. Demir, N. Gaponik and A. Eychmuller, *Nano letters*, 2012, 12, 5348-5354.
29. S. Kalytchuk, O. Zhovtiuk and A. L. Rogach, *Applied Physics Letters*, 2013, 103, 103105.
30. D. Geng, G. Li, M. Shang, C. Peng, Y. Zhang, Z. Cheng and J. Lin, *Dalton Transactions*, 2012, 41, 3078.
31. G. Li, Z. Hou, C. Peng, W. Wang, Z. Cheng, C. Li, H. Lian and J. Lin, *Advanced Functional Materials*, 2010, 20, 3446-3456.
32. R. Schmechel, M. Kennedy, H. von Seggern, H. Winkler, M. Kolbe, R. A. Fischer, L. Xiaomao, A. Benker, M. Winterer and H. Hahn, *Journal of Applied Physics*, 2001, 89, 1679-1686.
33. K. Riwozki and M. Haase, *The Journal of Physical Chemistry B*, 1998, 102, 10129-10135.
34. J. Chen, Q. Meng, P. S. May, M. T. Berry and C. Lin, *The Journal of Physical Chemistry C*, 2013, 117, 5953-5962.
35. C.-C. Tu, J.H. Hoo, K. F. Böhringer, L. Y. Lin and G. Cao, *Opt. Lett.*, 2012, 37, 4771-4773.
36. F. Liu, M. H. Jang, H. D. Ha, J. H. Kim, Y. H. Cho and T. S. Seo, *Adv Mater*, 2013, 25, 3657-3662.
37. J. Wang, J. Li and S.S. Li, *Journal of Applied Physics*, 2011, **110**, 054907.

38. X. Hu, J. C. Yu, J. Gong and Q. Li, *Crystal Growth & Design*, 2007, 7, 262-267.
39. J. Wang, S.-S. Li, Y. Liu and J. Li, *The Journal of Physical Chemistry C*, 2012, 116, 2 1039-21045.
40. A. Goldmann, J. Tejada, N. Shevchik and M. Cardona, *Physical Review B*, 1974, 10, 4388-4402.
41. E. Longo, E. Orhan, F. M. Pontes, C. D. Pinheiro, E. R. Leite, J. A. Varela, P. S. Pizani, T. M. Boschi, F. Lanciotti, A. Beltrán and J. Andrés, *Physical Review B*, 2004, 69, 125115.
42. B. L. Zhu and X. Z. Zhao, *Phys. Status Solidi A*, 2011, vol. 208, No. 1, 91–96.

Figure Captions:

Fig. 1 (a) XRD pattern of CuI nanophosphors for different reaction time representing the highly crystalline nature of the samples (b) High resolution XRD pattern of (111) peak demonstrating lower angle shift with gradual increase in the reaction time (c) Nanometer order size distribution of the CuI crystals (d) TEM image demonstrating the uniform dispersion of nanocrystalline CuI

Fig. 2 Representation of chemical shift in the high resolution XPS spectra of Cu 2p (a) and I 3d (b) core level of CuI nanophosphors (c) EDX pattern of CuI nanophosphors for different reaction times.

Fig. 3 (a) Room temperature PL spectra of the nanophosphors for different reaction time (b) HRTEM images of the nanophosphors showing the nature of lattice fringes (c) Calculated total density of states (TDOS) for the pure and interstitial iodine incorporated CuI structures

Fig. 4 (a) Optical images of the CuI nanophosphors irradiated under visible and UV light, respectively (b) chromaticity diagram representing the color coordinate of the corresponding red emission (c) UV-Visible transmittance spectra of the CuI films. Inset represents the overall transparency of the films demonstrated by placing it over the logo of Jadavpur University and bright emission of the same under 365 nm UV lamp

Fig. 5 Photoluminescence decay profiles of the nanophosphors for NBE and DLE, respectively

Fig. 6 (a) Polyhedral representation of crystal structure of CuI nanophosphors. Magnified view of one unit cell that contains two excess iodines in octahedral positions is also shown. (b) partial density of states (PDOS) of the pure and (c) interstitial iodine incorporated CuI structures.

Fig. 7 (a)&(b) Demonstration of prototype light emitting device operated under an applied voltage 3 Volt. (c) Electroluminescence spectra of the device recorded under different applied

voltage. (d) Color coordinate of the emitted radiation at different applied voltage demonstrated in CIE chromaticity diagram with respect to HDTV standard color triangle.

Figures:

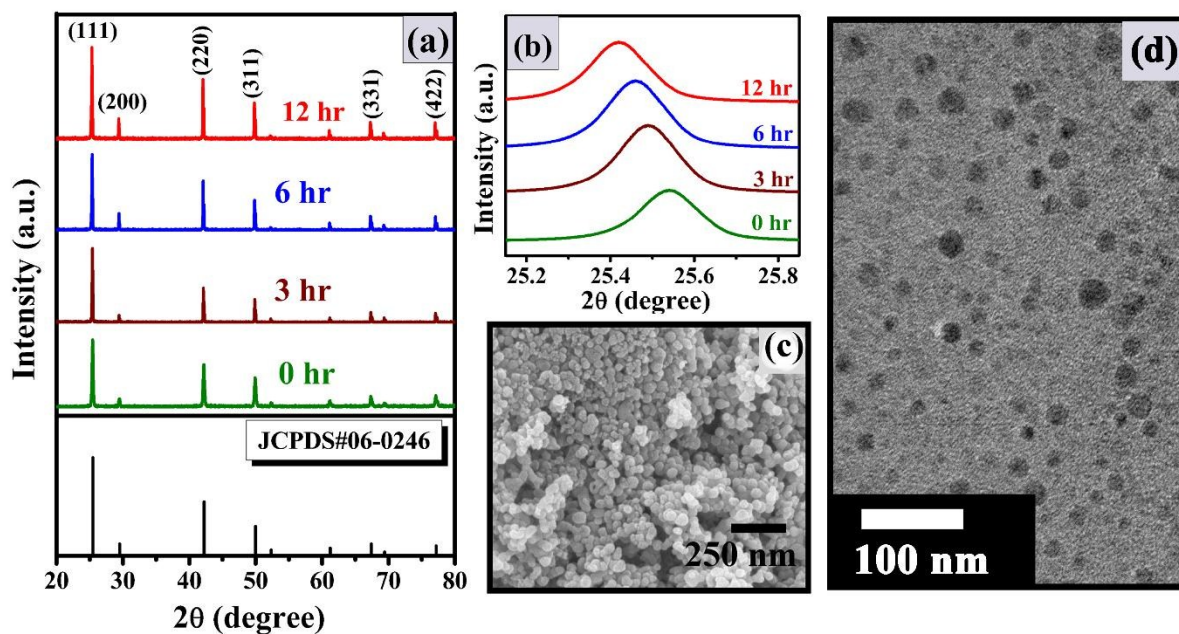


Figure 1

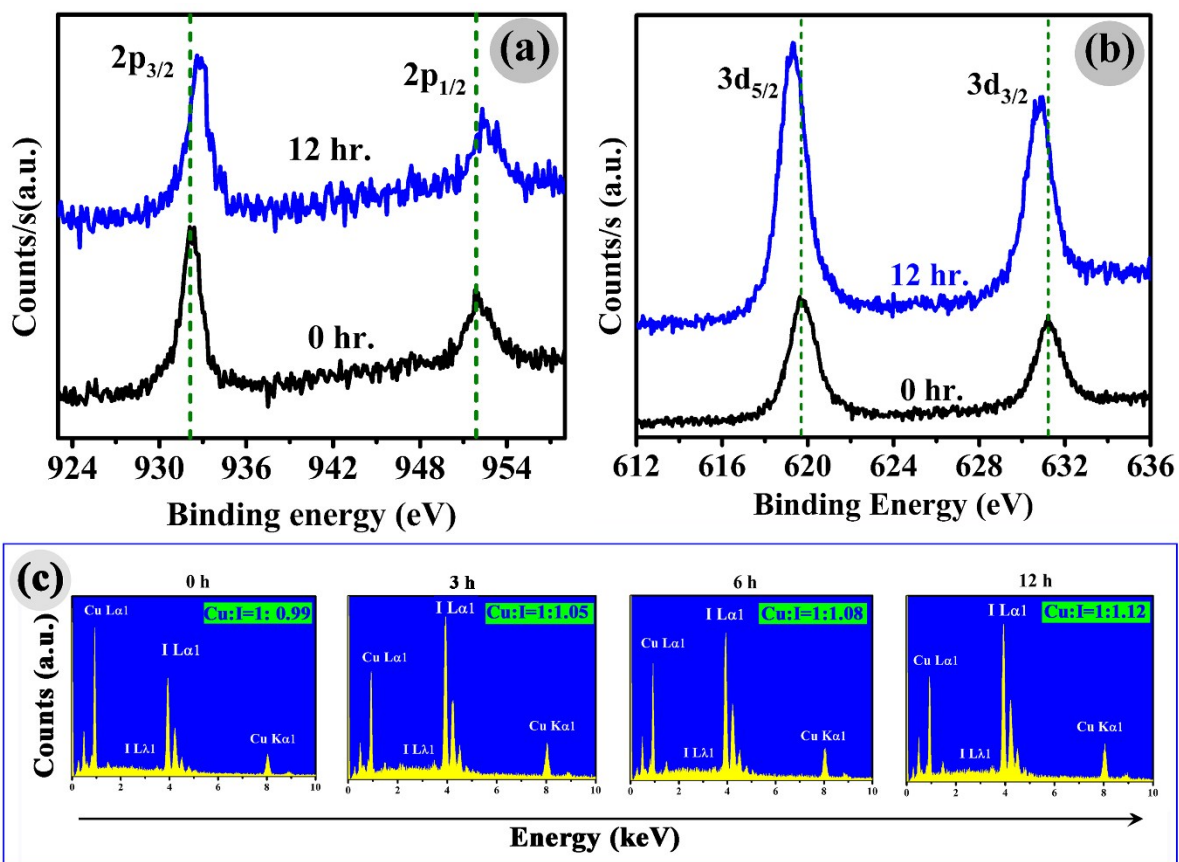


Figure 2

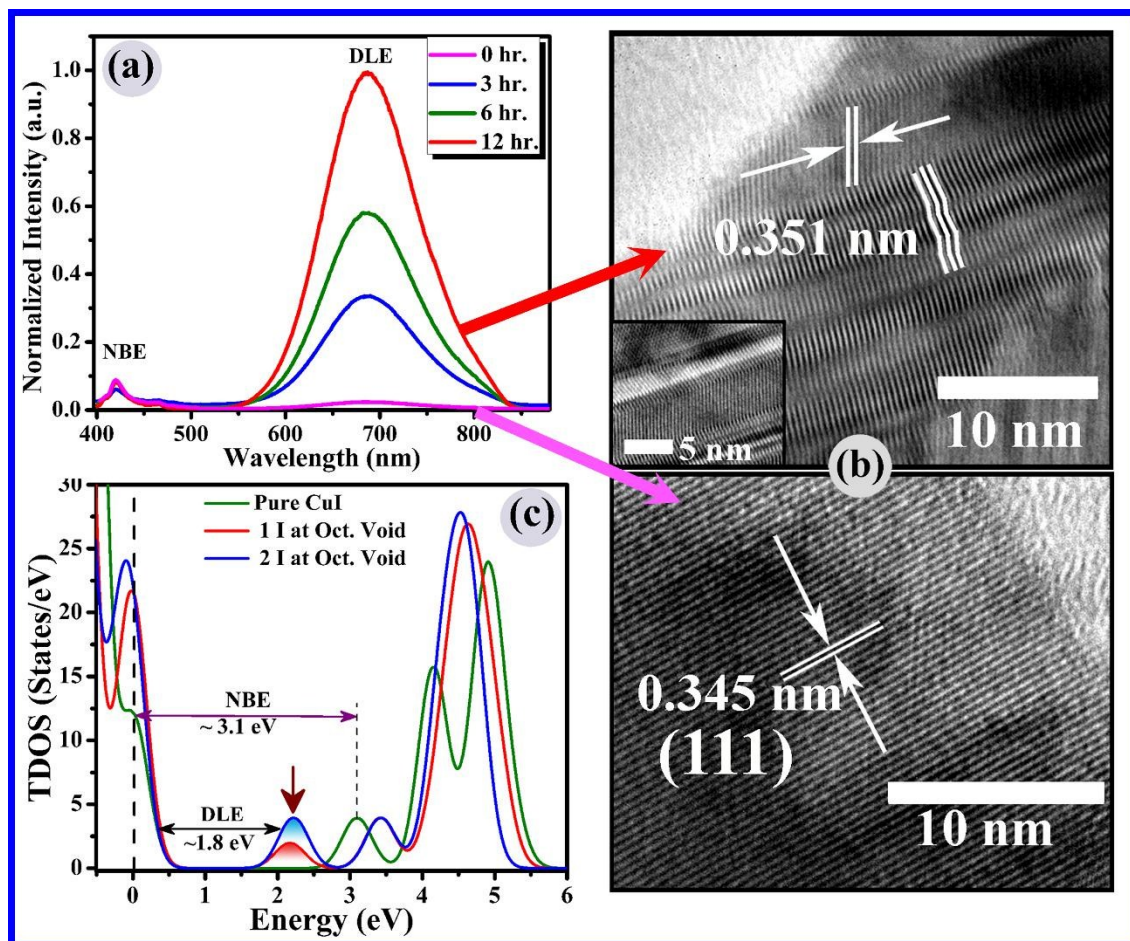


Figure 3

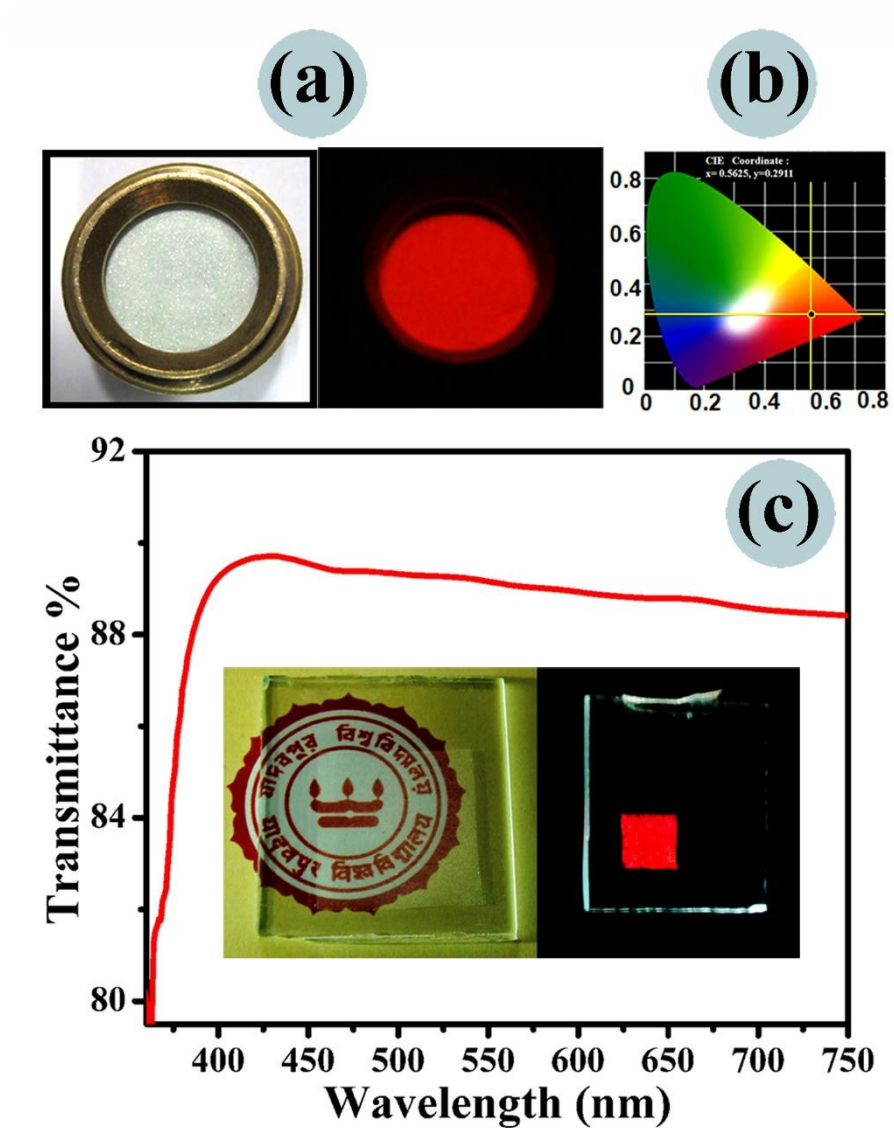


Figure 4

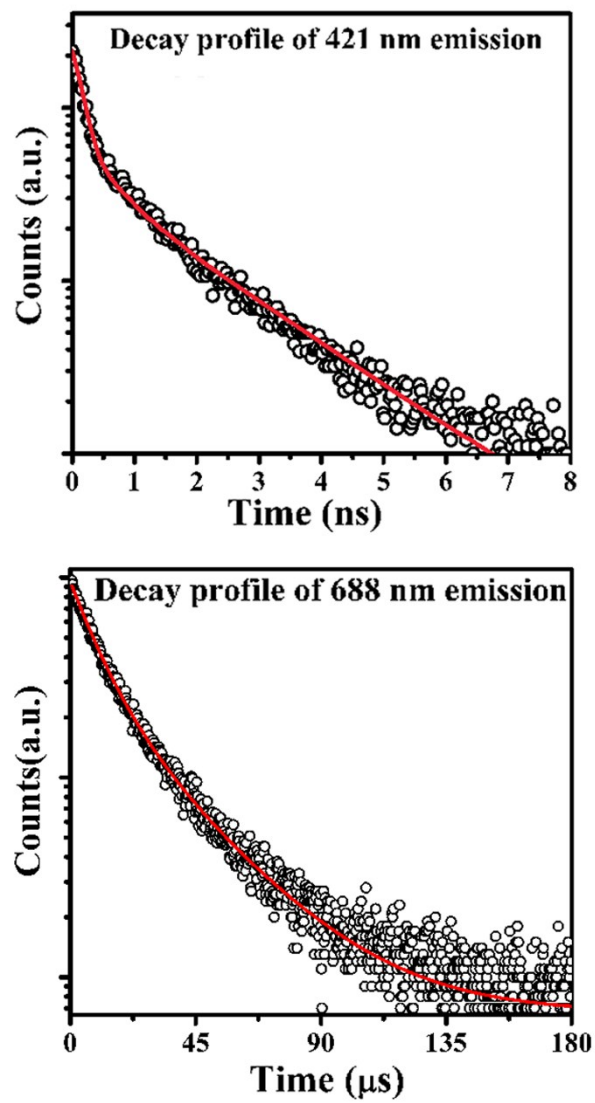


Figure 5

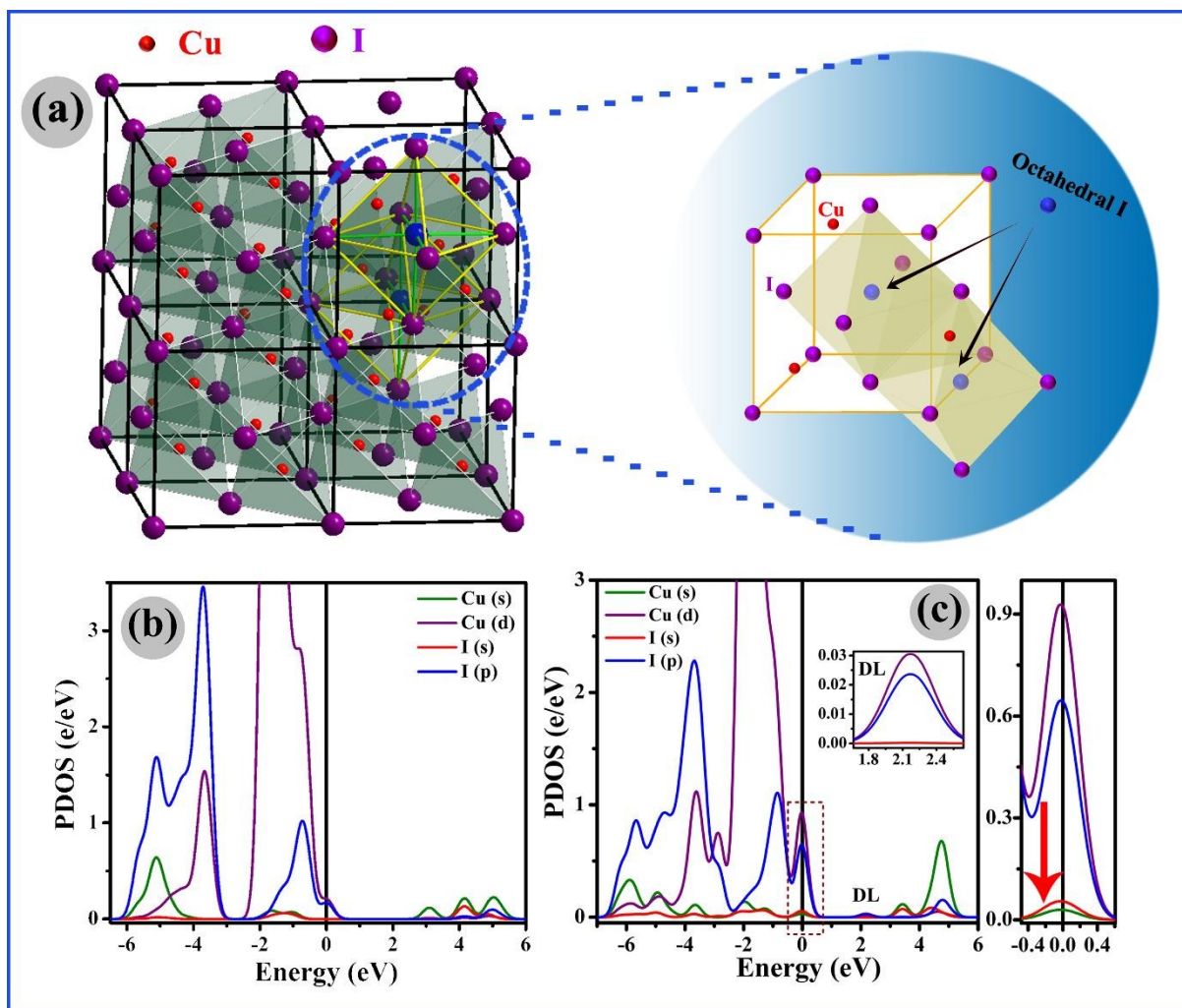


Figure 6

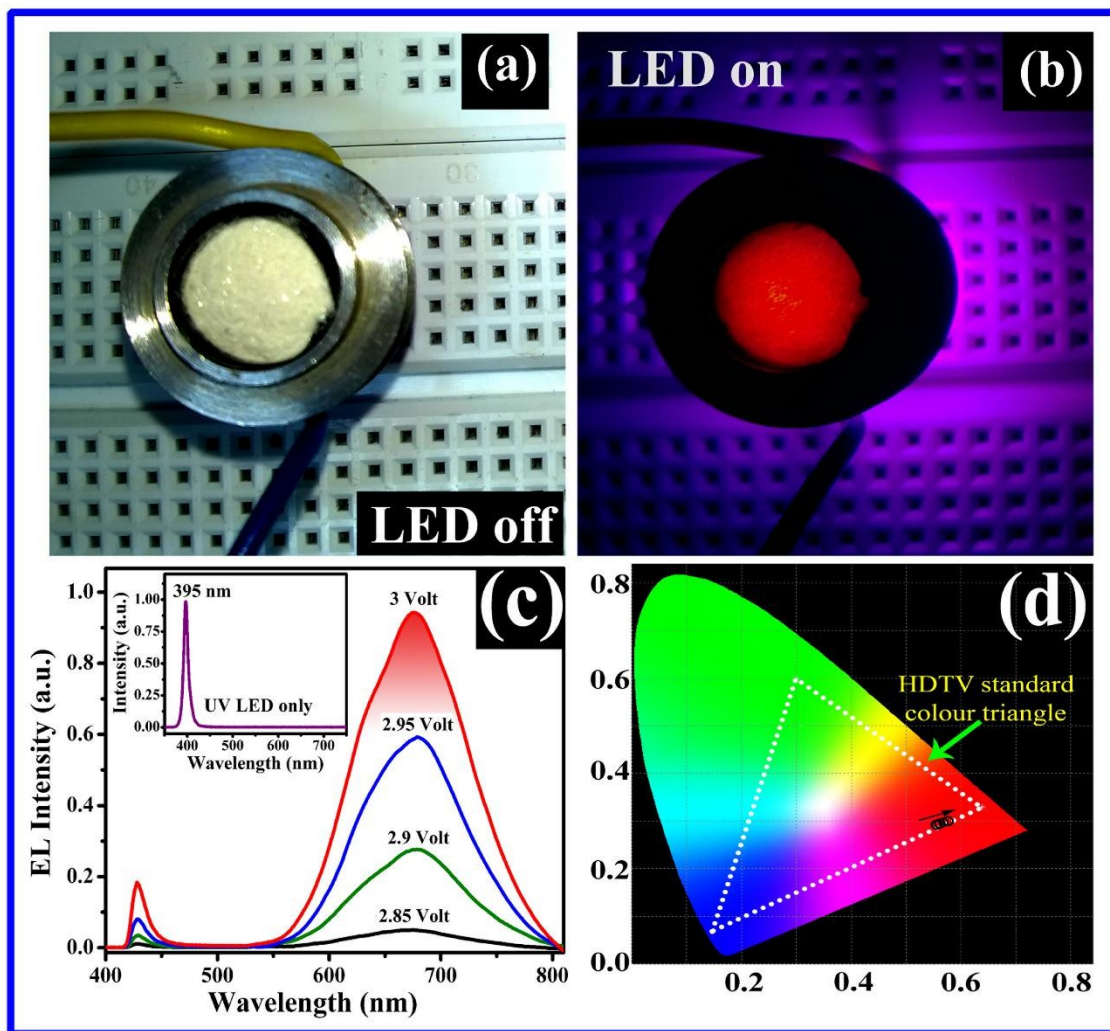
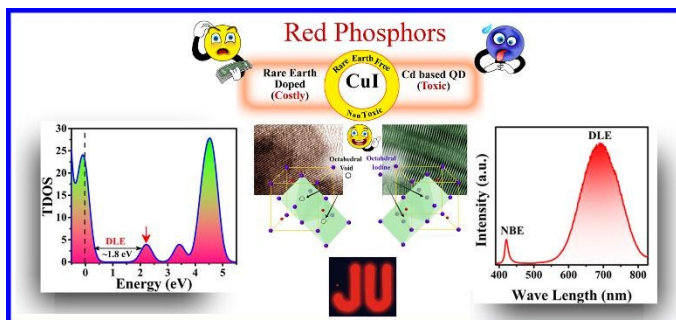


Figure 7

Table 1: Comparison of PL properties of CuI nanophosphors with some already existing conventional red nanophosphors

Nanophosphor type	Excitation wavelength (nm)	Emission wavelength (nm)	PL Quantum Yield (%)	Remarks	Ref.
Y ₂ O ₃ :Eu ³⁺ nanophosphor	253 nm	611 nm	10% (in solid)	Costly, Due to low excitation wavelength not suitable for WLED	32
YVO ₄ :Eu ³⁺ nanophosphor	310 nm	618 nm	15% (in solution)	Costly, Due to low excitation wavelength not suitable for WLED	33
YPO ₄ :Eu ³⁺ nanophosphor	350 nm	613 nm	0.31% (in solution)	Costly, poor quantum yield	34
CdTe quantum dot	385 nm	652 nm	15% (in solid)	Highly toxic	29
CdS:Cu quantum dot	460 nm	663 nm	18%-30% (in solution)	Highly toxic	27
Si quantum dot	405 nm	630 nm	17% (in solution)	Low stability	35
CuI nanophosphor	397 nm	688 nm	21% (in solid)	Ecofriendly, nontoxic, stable	[This work]

Table of contents graphics:

Ultra high red luminescence is demonstrated from rare earth free as well as non-toxic cuprous iodide nanophosphors. Going beyond to the initial stoichiometry, intentional incorporation of excess iodine in CuI lattice generates defect center mediated strong red emission which can be implemented directly in the field of advanced energy saving lighting applications.